nature physics

Article

https://doi.org/10.1038/s41567-022-01846-y

Bosonic stimulation of atom–light scattering in an ultracold gas

Received: 14 July 2022

Accepted: 18 October 2022

Published online: 22 December 2022

Check for updates

Yu-Kun Lu ✉, Yair Margalit & Wolfgang Ketterle

For bosons, the transition rate into an already occupied quantum state is enhanced by its occupation number: the effect of bosonic stimulation. Bosonic stimulation of light scattering was predicted more than 30 years ago but has proven elusive to direct observation. Here we investigate this effect in an ultracold gas of bosons. We show that the bosonic enhancement factor for a harmonically trapped gas is bounded by a universal constant above the phase transition to a Bose–Einstein condensate and depends linearly on the condensate fraction just below the phase transition. We observe bosonic enhanced light scattering both above and below the phase transition, and we show how interactions can alter the bosonic stimulation and optical properties of the gas. Lastly, we demonstrate that, for a multi-level system prepared in a single internal state, the bosonic enhancement is reduced because it occurs only for Rayleigh scattering but not for Raman scattering.

Bosonic stimulation occurs for bosonic particles transitioning into a final state with non-zero occupation number n, where the transition rate is enhanced by a factor of $n+1$. Since most elementary particles are fermions, most observations of bosonic stimulation have been related to photons, with the laser as the most dramatic manifestation. The field of ultracold atoms has created new opportunities to realize other paradigmatic phenomena for bosonic stimulation. It has been observed in the formation of Bose–Einstein condensate (BEC)[1] and enhanced density fluctuations[2,3]. Bosonic stimulation can also lead to super-radiance[4] and matter-wave amplification[5,6]. However, these phenomena occur also for non-condensed thermal clouds, and for fermions and distinguishable particles, are therefore not directly connected to quantum statistics (Supplementary Information and refs. [7–10]). They have a mainly classical origin and can all be traced back to the diffraction of light from a periodic density modulation, which in the case of Rayleigh super-radiance is created by a strong light pulse (Supplementary Information). The basic phenomenon of bosonic enhancement of light scattering which occurs in a gas in thermal equilibrium, although predicted more than 30 years ago, has not been observed before[11–17]. One previous, unsuccessful attempt to observe bosonically enhanced light scattering monitored the loss of atoms[18], whereas here we detect the scattered light directly. One reason why such experimental observation has been elusive[18,19] is the requirement for temperatures comparable to or higher than the recoil temperature. Quantum degeneracy at such temperatures implies high densities in the range of one or more atoms per $\lambda\!\!\!^{-3}$ (where $\lambda\!\!\!^{-} = \lambda/2\pi$ is the reduced wavelength). At such densities, ultracold atomic clouds become short-lived due to inelastic collisions[20,21]. For the same reason, the fermionic counterpart (Pauli blocking of light scattering) was demonstrated only very recently[19,22,23].

In this work, we theoretically investigate and experimentally observe bosonic enhancement of light scattering in an ultracold Bose gas of sodium atoms. We obtain new analytic results for the enhancement factor for non-interacting bosons in several regimes. Experimentally, we prepared a dense cloud of bosons with a peak density of up to 2×10^{15} cm^{-3} and a BEC transition temperature of $T\approx10$ μK, achieving the highest critical density in ultracold atoms including spin-polarized hydrogen. The bosonic enhancement of light scattering was observed in two different regimes: for scattering within the thermal cloud, and for scattering between the BEC and thermally occupied states. We show how interactions modify the bosonic stimulation by modifying the overlap between the condensate and thermal cloud and by changing the pair correlation function.

The principle behind bosonic stimulation in light scattering is illustrated in Fig. 1. Light scattering is a two-photon process in which an atom absorbs a photon (with momentum $\mathbf{k}_i$) from the probe beam and emits a scattered photon (momentum $\mathbf{k}_f$). The momentum of the atom changes due to the photon recoil by $\mathbf{q}=\mathbf{k}_i-\mathbf{k}_f$ (Fig. 1a). In general, the (normalized) light scattering rate is given by the structure

Research Laboratory of Electronics, MIT-Harvard Center for Ultracold Atoms, Department of Physics, Massachusetts Institute of Technology, Cambridge, MA, USA. ✉e-mail: yukunlu@mit.edu

https://doi.org/10.1038/s41567-022-01846-y

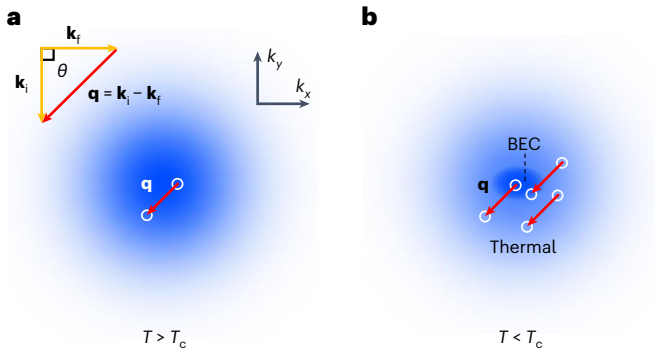

Fig. 1 | Schematic of bosonic stimulation in light scattering. Momentum-space pictures of the cloud above and below the phase transition. When a photon is scattered, the photon recoil changes the momentum of the atom by **q** (red arrow). **a**, Above the phase transition ($T > T_c$), both the initial and final momentum states are in the thermal cloud. **b**, Below the phase transition ($T < T_c$), a condensate emerges around zero momentum, and scattering between the condensate and the thermal cloud is also possible. In either case, light scattering is enhanced if the final state is occupied.

factor, which can be obtained in the local density approximation by averaging over the phase space[24]:

$$S(\mathbf{q}) = 1 \pm \langle n(\mathbf{r}, \mathbf{p} + \mathbf{q}) \rangle, \tag{1}$$

where the plus (minus) sign corresponds to bosons (fermions). The phase-space average is weighted by the occupation number $n(\mathbf{r}, \mathbf{p})$. In the limit of zero recoil momentum, the second term reduces to the average phase-space density (PSD). This term becomes 1 for fermions at zero temperature, predicting complete Pauli blocking[22]. For bosons, the physics is richer because of the presence of the BEC phase transition. For a non-degenerate thermal gas, the averaged PSD is $n\lambda_t^3/2^{3/2}$ (where n is the density and λ_t is the thermal de Broglie wavelength). Extrapolating this formula to the BEC phase transition with the criterion $n\lambda_t^3 = \zeta(3/2) \approx 2.612$ gives an enhancement factor of 1.92 (where ζ is the Riemann zeta function). However, we will show that the enhancement factor at the transition temperature can diverge (in free space) or is limited to $\zeta(2)/\zeta(3) \approx 1.37$ for harmonic confinement.

The phase-space occupation number $n(\mathbf{r}, \mathbf{p})$ in equation (1) is given by the Bose–Einstein occupation number in the thermal cloud $n_{th} = \left[\exp\left[(\epsilon_{\mathbf{p}} + U(\mathbf{r}) - \mu)/k_B T\right] - 1\right]^{-1}$. The presence of a non-interacting condensate adds a δ function in phase space:

$$n(\mathbf{r}, \mathbf{p}) = \begin{cases} n_{th}(\mathbf{r}, \mathbf{p}) & T \geq T_c \\ n_{th}(\mathbf{r}, \mathbf{p})|_{\mu=0} + h^3 N_0 \delta(\mathbf{r}, \mathbf{p}) & T < T_c \end{cases}. \tag{2}$$

Here $\epsilon_{\mathbf{p}} = p^2/2m$, $U(\mathbf{r})$ and μ represent the kinetic energy, potential energy, and chemical potential, respectively. $N_0 = f(T/T_c)N$ is the number of atoms in the condensate, with f being the condensate fraction and h being Planck's constant.

Above T_c, scattering occurs between two thermally occupied states (Fig. 1a). The scattering rate is enhanced as the temperature approaches T_c because of the increase of $n_{th}(\mathbf{r}, \mathbf{p})$ at low momenta. Below the transition temperature, scattering into and out of the condensate becomes possible (Fig. 1b). Combining the expression for $n(\mathbf{r}, \mathbf{p})$ with equation (1), the total scattering rate below T_c reads

$$S(\mathbf{q}) = 1 + 2f n_{th}(0, \mathbf{q}) + \langle n_{th}(\mathbf{r}, \mathbf{p} + \mathbf{q})|_{\mu=0} \rangle. \tag{3}$$

The first term represents the contribution of single-particle Rayleigh scattering events, the second term denotes the condensate-to-thermal scattering events and the third term describes thermal-to-thermal scattering events. For a harmonically trapped Bose gas, the scattering is dominated by scattering events involving the condensate already for moderate condensate fractions. As the temperature becomes lower, the condensate fraction f increases but the occupation number $n_{th}(0, \mathbf{q})$ ($n_{th}(0, \mathbf{q}) \approx k_B T/E_{rec}$ for $k_B T \gg E_{rec}$) in the thermal cloud decreases. As a result, the total scattering rate first increases and then decreases as the temperature is further decreased below T_c. Ultimately, at zero temperature, all the atoms are in the condensate and bosonic stimulation is absent because of the zero occupation of the final states. Figure 2b shows the theoretical calculation for a non-interacting Bose gas in a harmonic trap.

Bosonic enhancement increases monotonically as the (normalized) recoil momentum $\kappa = \sqrt{E_{rec}/k_B T_c}$ decreases (where $E_{rec} = q^2/2m$ is the atomic recoil energy). In a harmonic trap, for $\kappa \to 0$, the enhancement above the BEC phase transition is bounded by $\zeta(2)/\zeta(3) \approx 1.37$, while the enhancement factor below T_c diverges as $1/\kappa^2$. In contrast, in free space (with a three-dimensional (3D) box potential), the enhancement factor diverges as $\pi^{3/2}\kappa^{-1}/\zeta(3/2)$ already at $T = T_c$. This major difference illustrates that, in a harmonic trap at T_c, only a small volume is at or near the conditions for the phase transition. A derivation of these results, as well as a generalization to arbitrary power-law potentials, can be found in Methods.

In the experiment, around 4×10^5 partially condensed ^{23}Na atoms in the hyperfine state $|F = 2, m_F = 2\rangle$ are prepared in an optical dipole trap (Methods). The cloud is then heated up to different temperatures by modulating the trap intensity while keeping the atom number almost constant. Light is scattered by exciting the cycling transition with σ_+-polarized light. Due to the large detuning $\Delta = 25.7$ GHz (or 2,600 linewidths Γ), shifts and broadenings due to dipolar interactions are negligible. The optical setup is described in ref. [22]. For the measurements to be perturbative, the scattering rate was kept below 0.08 photons per atom during 4 ms. We observed light scattering for four different densities over a range of temperatures (Fig. 2a). The density is controlled by adjusting the depth of the optical dipole trap and determines T_c and κ. The red line in Fig. 2 shows the parameters of these measurements (where the traces for the different values of T_c overlap).

The data in Fig. 2, even without quantitative analysis, show the salient features of light scattering for bosons. Above the phase transition, there is a modest enhancement in scattering due to the increase in the phase-space density as the temperature is reduced. Once the condensate forms, the enhancement is more substantial due to scattering into and out of the condensate. We also observed the absence of enhanced light scattering for an almost pure Bose–Einstein condensate. However, due to the strong increase of three-body losses at high density, we could prepare such condensates only at lower densities in more weakly confining traps where the maximum enhancement is small owing to the larger value of κ. When the cloud was compressed to higher densities (Fig. 2b, black trajectory), an increase of light scattering was observed, qualitatively consistent with the prediction (Methods).

For temperatures above T_c, light scattering occurs within the thermal distribution. In Fig. 3a, we compare the results with the predictions for an ideal gas and an interacting gas, without any free parameters except the overall scaling. Data with different T_c are binned together because of their small difference in κ. Usually, thermal Bose gases away from Feshbach resonances are treated as non-interacting. However, at our high densities, the mean-field (MF) repulsion is relevant even for thermal clouds. It softens the trapping potential and increases the bosonic enhancement by up to 50% because of the higher density of states at low energy (Methods). Bosonic stimulation is reduced by a second effect of interactions: the reduction of the pair correlation function suppresses the enhancement by a factor $1 - 8\sqrt{2}a/\lambda_t \approx 0.6$ at high temperatures (where a is the s-wave scattering length)[25] (Methods). Close to the phase transition, the thermal de Broglie

https://doi.org/10.1038/s41567-022-01846-y

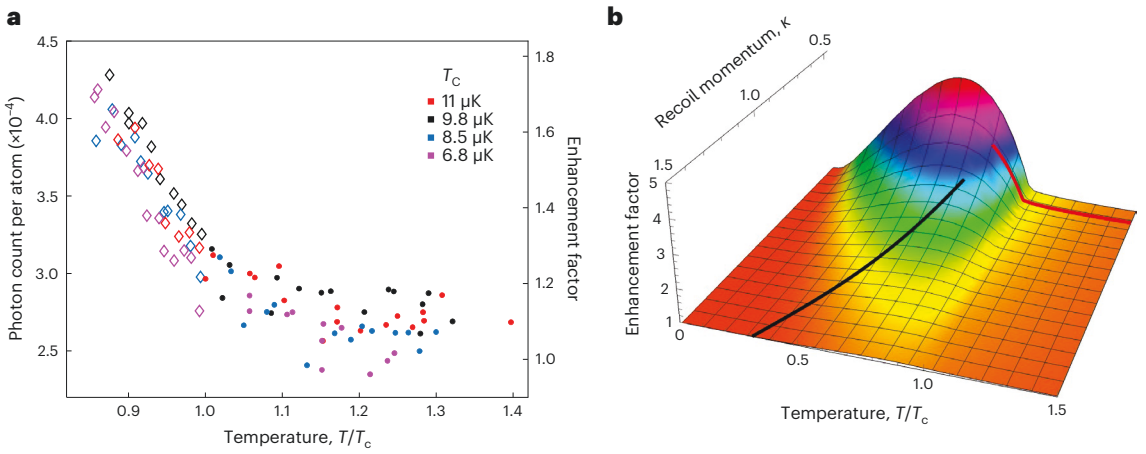

Fig. 2 | Bosonic stimulation of light scattering in a trapped ^{23}Na gas across the phase transition. a, Experimental data of light scattering versus temperature at different densities (different colours) above (dots) and below (diamonds) the phase transition. Data points here are each averaged over 12–16 samples. The vertical uncertainty is reflected by the scatter of the data, while the horizontal error is around 2%. The error bars throughout the whole paper are purely statistical and reflect the s.e.m. **b**, Theoretical prediction of the bosonic enhancement factor for a harmonically trapped non-interacting gas, corresponding to the traces in **a** (red trajectory) or when an almost pure condensate is prepared at low density and compressed (black trajectory).

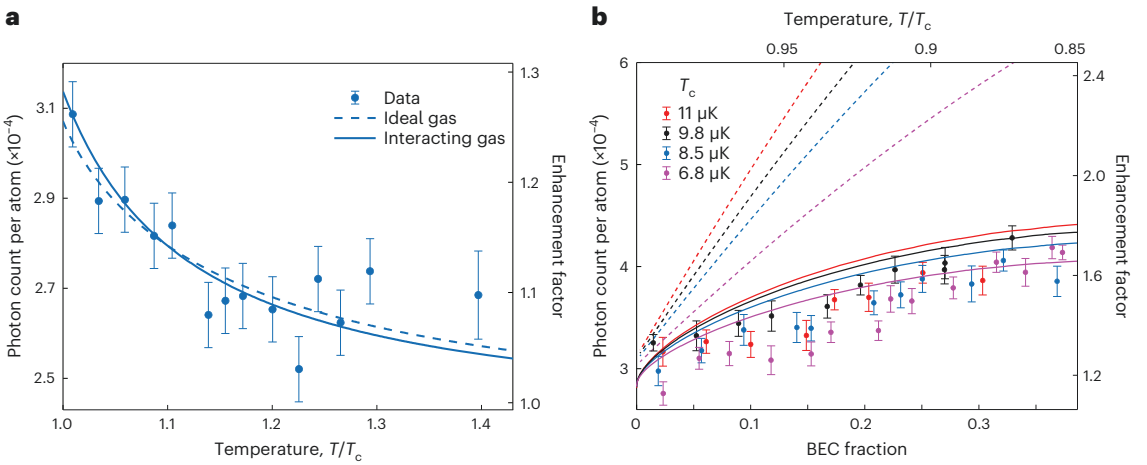

Fig. 3 | Bosonic enhancement of light scattering above and below the BEC phase transition. a, Above the phase transition, scattering occurs within the thermal cloud. The dashed curve represents the theoretical prediction for ideal gas, while the solid curve represents the interacting theory. The interaction effect appears to be small, but this is due to coincidental cancellation between the contributions from the MF effect and pair correlations. The data are identical to those in Fig. 2 with $T > T_c$ but averaged over nearby points. The error along the temperature axis is around 2%. **b**, Below the phase transition, the scattering between the BEC and thermal cloud dominates. The dashed curves are predictions for ideal gas, while the solid curves use a semi-ideal gas approximation and the modified pair correlation function. The data are identical to those in Fig. 2 with $T < T_c$.

wavelength λ_t is effectively replaced by the correlation length ξ. The divergence of ξ at the phase transition will diminish the suppression caused by pair correlation. To the best of the authors' knowledge, the suppression of bosonic stimulation by repulsive interactions has not been discussed before. In Methods, we discuss some evidence for the effect of pair correlations. Figure 3a demonstrates that the two effects of interactions almost cancel each other.

For temperatures below the BEC phase transition, the scattering between the condensate and the thermal cloud dominates the bosonic enhancement. For a non-interacting Bose gas, the enhancement factor increases almost linearly with the condensate fraction close to the critical point: $S(\mathbf{q}) \approx 1 + 2fk_B T/E_{rec}$ (Fig. 3b, dashed curves). However, because of the MF repulsion between the thermal cloud and the condensate, the density of thermal atoms inside the condensate volume is strongly reduced[26], diminishing the bosonic enhancement. The enhancement $S(\mathbf{q}) - 1$ is thus reduced by the factor $(\int \mathrm{d}\mathbf{r}\, n_0(\mathbf{r}) n_{th}^{(int)}(\mathbf{r}, \mathbf{q}))/(N_0 n_{th}(0, \mathbf{q}))$, with $n_0(\mathbf{r})$ being the density distribution of the interacting BEC, and $n_{th}^{(int)}(\mathbf{r}, \mathbf{q})$ the phase-space occupation number for the interacting thermal cloud. The experimentally observed enhancement is reduced by up to a factor of 3 compared with the non-interacting theory (Fig. 3b). We model the effect of interactions using the semi-ideal gas approximation[26], which assumes an interacting condensate and repulsion of the thermal cloud by the condensate, and include the modified pair correlation function[25] (Fig. 3b). Note that the theoretical curves in Fig. 3b have no free parameters (the overall scaling being the same as in Fig. 3a). Our model explains most of the reduction in light scattering compared with the predictions for a non-interacting gas. The remaining difference could be due to the back-action from the thermal cloud to the BEC, which will further reduce their overlap and can be treated approximately using a Hartree–Fock approximation (Methods). However, a fully consistent treatment of the interacting Bose gas is challenging both theoretically and numerically. Note that,

https://doi.org/10.1038/s41567-022-01846-y

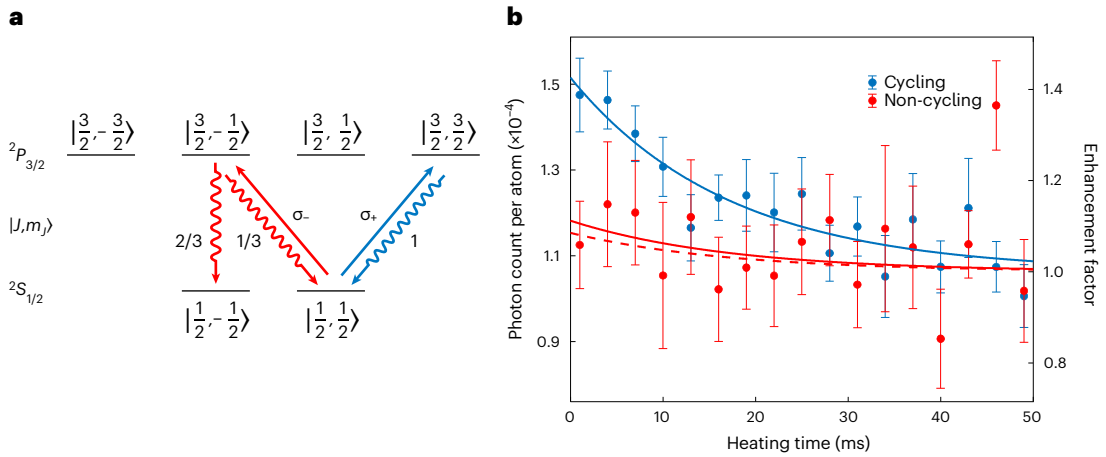

Fig. 4 | Bosonic enhancement for Rayleigh and Raman scattering. a, For large detuning, the atom's internal states are labelled by $|J, m_J\rangle$, where J represents the total angular momentum of the electron and m_J its projection along the quantization axis. The blue (red) straight arrow represents the excitation paths for probe light with σ_+ (σ_-) polarization, while the wavy arrows represent the emitted photons with branching ratio labelled on the side. **b**, Observed photon scattering for σ_+ (blue) and σ_- (red, scaled by 9/5) polarized probe light. The solid blue curve is a fit to the σ_+ data (using an exponential function as a convenient trial function), the red dashed line is obtained from the blue fit and equation (4). The solid red line is a fit to equation (4) with adjustable γ. Each data point is an average over 12 samples.

for an interacting condensate, light scattering can be strongly modified by the spectrum of collective excitations. For example, for momentum transfers which create phonons, light scattering is suppressed[27].

Until now, we have assumed a two-level system, realized by exciting the initial $|F = 2, m_F = 2\rangle$ hyperfine state on a cycling transition with σ_+-polarized light (Fig. 4a, blue). We now discuss the situation in which the atoms are excited with light of different polarization. In the limit of detunings much larger than the hyperfine interaction in the excited state, the nuclear hyperfine structure can be neglected since the nuclear spin state does not change during the light scattering. Therefore, we realize the simplified level diagram shown in Fig. 4a.

When the atoms are initially prepared in a single internal state, only Rayleigh scattering shows bosonic enhancement. Raman scattering (or optical pumping) populates initially empty states and is not enhanced. We therefore expect the enhancement factor η to be reduced to $\gamma\eta + (1-\gamma)$, where γ represents the branching ratio (the ratio of Rayleigh scattering to Raman scattering). To describe our experimental situation, we express the observed scattering rate for σ_+ light as $R_+ = \eta R$, with R representing the Rayleigh scattering rate without any enhancement. The expected observed scattering rate for σ_- light is then predicted as

$$R_- = \frac{1}{3}(\gamma\eta R + 2(1-\gamma)R). \quad (4)$$

Here, the prefactor of 1/3 results from the reduced matrix element, the branching ratio of $\gamma = 1/3$, and an extra factor of 2 from the different angular distributions for the scattered σ and π light. By comparing equation (4) in the high-temperature and low-temperature limit, we find the enhancement factor for σ_- polarized light to be $(4+\eta)/5$. The results presented in Fig. 4b confirm that the bosonic enhancement for σ_- probe light is always below the enhancement for σ_+. We can use equation (4) and regard γ as a fitting parameter that characterizes the bosonic enhancement. The best fit to the data gives $\gamma = 0.4(2)$ and is consistent with the theoretical prediction ($\gamma = 1/3$) within the experimental uncertainty (which is larger for σ_- scattering owing to the small number of photons observed). If the light scattering is non-perturbative, the population can build up in the initially empty state via optical pumping, which will then lead to super-radiantly enhanced Raman scattering[28,29].

In conclusion, we have shown how quantum statistics and interaction modifies the optical properties of a Bose gas. We have worked in a regime where the effect of quantum statistics dominates over other effects such as dipole–dipole interactions[30], super-radiance[4], light-assisted collisions[31], multiple scattering and atomic lensing. Super-radiance is another form of enhanced light scattering but is not directly connected to quantum statistics. It is caused by coherence (in the form of symmetric Dicke states[32]). These coherences are created by light–atom interactions due to non-linear light scattering. In contrast, our experiment was done in the perturbative limit and probed the quantum statistical pair correlations of an equilibrium quantum gas. Besides the fundamental interest, understanding light scattering is crucial for quantitative diagnostics of bosonic systems. For future work, it would be promising to study bosonic enhancement of light scattering in a box potential[33] because of the absence of density inhomogeneity. The large extension of the critical region will give much stronger enhancement and enable studies of the $1/\kappa$ divergence of the enhancement factor. In addition, in a box potential, interactions can affect light scattering only through the modification of the pair correlation function. It should be possible to clearly observe how bosonic enhancement is reduced above the phase transition, but not right at the critical point. Furthermore, for strong repulsive interactions near a Feshbach resonance, light scattering in bosons could possibly be even suppressed below the single-particle Rayleigh rate, in analogy with Pauli blocking for fermions. Both Pauli blocking and strong interactions reduce the pair correlation function. More generally, light scattering provides a way to measure the static structure factor, which could be used to characterize strongly interacting systems, including systems with strong dipolar interactions which are anisotropic and long range.

Online content

Any methods, additional references, Nature Portfolio reporting summaries, source data, extended data, supplementary information, acknowledgements, peer review information; details of author contributions and competing interests; and statements of data and code availability are available at https://doi.org/10.1038/s41567-022-01846-y.

References

1. Miesner, H.-J. et al. Bosonic stimulation in the formation of a Bose–Einstein condensate. *Science* **279**, 1005–1007 (1998).

2. Esteve, J. et al. Observations of density fluctuations in an elongated Bose gas: ideal gas and quasicondensate regimes. *Phys. Rev. Lett.* **96**, 130403 (2006).
3. Blumkin, A. et al. Observing atom bunching by the Fourier slice theorem. *Phys. Rev. Lett.* **110**, 265301 (2013).
4. Inouye, S. et al. Superradiant Rayleigh scattering from a Bose–Einstein condensate. *Science* **285**, 571–574 (1999).
5. Inouye, S. et al. Phase-coherent amplification of atomic matter waves. *Nature* **402**, 641–644 (1999).
6. Kozuma, M. et al. Phase-coherent amplification of matter waves. *Science* **286**, 2309–2312 (1999).
7. Moore, M. G. & Meystre, P. Atomic four-wave mixing: fermions versus bosons. *Phys. Rev. Lett.* **86**, 4199–4202 (2001).
8. Ketterle, W. & Inouye, S. Does matter wave amplification work for fermions? *Phys. Rev. Lett.* **86**, 4203–4206 (2001).
9. Yoshikawa, Y., Torii, Y. & Kuga, T. Superradiant light scattering from thermal atomic vapors. *Phys. Rev. Lett.* **94**, 083602 (2005).
10. Wang, P. et al. Observation of collective atomic recoil motion in a degenerate fermion gas. *Phys. Rev. Lett.* **106**, 210401 (2011).
11. Svistunov, B. & Shlyapnikov, G. Resonance optics of the low-temperature quantum gases H and D. *Sov. Phys. JETP* **70**, 460–466 (1990).
12. Politzer, H. D. Light incident on a Bose-condensed gas. *Phys. Rev. A* **43**, 6444–6446 (1991).
13. Zhang, W. & Walls, D. F. Quantum field theory of interaction of ultracold atoms with a light wave: Bragg scattering in nonlinear atom optics. *Phys. Rev. A* **49**, 3799–3813 (1994).
14. Morice, O., Castin, Y. & Dalibard, J. Refractive index of a dilute Bose gas. *Phys. Rev. A* **51**, 3896–3901 (1995).
15. Javanainen, J. & Ruostekoski, J. Off-resonance light scattering from low-temperature Bose and Fermi gases. *Phys. Rev. A* **52**, 3033–3046 (1995).
16. Javanainen, J. Optical signatures of a tightly confined Bose condensate. *Phys. Rev. Lett.* **72**, 2375–2378 (1994).
17. Politzer, H. D. Bose-stimulated scattering off a cold atom trap. *Phys. Rev. A* **55**, 1140–1146 (1997).
18. Bons, P. C., de Haas, R., de Jong, D., Groot, A. & van der Straten, P. Quantum enhancement of the index of refraction in a Bose–Einstein condensate. *Phys. Rev. Lett.* **116**, 173602 (2016).
Claimed the observation of bosonic enhancement of light scattering. However, their observable was atom loss caused by optical pumping. As we show in the last part of the paper, optical pumping (that is, Raman scattering) into an unoccupied state does not show any bosonic enhancement. Instead, the observed loss could be caused by inelastic collisions or non-linear light scattering.
19. Deb, A. B. & Kjærgaard, N. Observation of Pauli blocking in light scattering from quantum degenerate fermions. *Science* **374**, 972–975 (2021).
After the experimental work had been completed and presented at the BEC 2021 conference, possible evidence of bosonic stimulation effects was observed in optical absorption measurements which showed an enhancement of 10–15% across the BEC phase transition. However, this effect was explained without considering light scattering involving the condensate, and no full analysis was given (since the topic of the paper was Pauli blocking for fermions).
20. Inguscio, M., Stringari, S. & Wieman, C. *Bose–Einstein Condensation in Atomic Gases*, vol. 140 (IOS Press, 1999).
21. Top, F. Ç., Margalit, Y. & Ketterle, W. Spin-polarized fermions with p-wave interactions. *Phys. Rev. A* **104**, 043311 (2021).
22. Margalit, Y., Lu, Y.-K., Çağrı Top, F. & Ketterle, W. Pauli blocking of light scattering in degenerate fermions. *Science* **374**, 976–979 (2021).
23. Sanner, C. et al. Pauli blocking of atom-light scattering. *Science* **374**, 979–983 (2021).
24. Shuve, B. & Thywissen, J. Enhanced Pauli blocking of light scattering in a trapped Fermi gas. *J. Phys. B* **43**, 015301 (2009).
25. Naraschewski, M. & Glauber, R. J. Spatial coherence and density correlations of trapped Bose gases. *Phys. Rev. A* **59**, 4595–4607 (1999).
26. Naraschewski, M. & Stamper-Kurn, D. M. Analytical description of a trapped semi-ideal Bose gas at finite temperature. *Phys. Rev. A* **58**, 2423–2426 (1998).
27. Stamper-Kurn, D. M. et al. Excitation of phonons in a Bose-Einstein condensate by light scattering. *Phys. Rev. Lett.* **83**, 2876–2879 (1999).
28. Schneble, D. et al. Raman amplification of matter waves. *Phys. Rev. A* **69**, 041601 (2004).
29. Yoshikawa, Y., Sugiura, T., Torii, Y. & Kuga, T. Observation of superradiant Raman scattering in a Bose–Einstein condensate. *Phys. Rev. A* **69**, 041603 (2004).
30. Zhu, B., Cooper, J., Ye, J. & Rey, A. M. Light scattering from dense cold atomic media. *Phys. Rev. A* **94**, 023612 (2016).
31. Weiner, J., Bagnato, V. S., Zilio, S. & Julienne, P. S. Experiments and theory in cold and ultracold collisions. *Rev. Mod. Phys.* **71**, 1–85 (1999).
32. Dicke, R. H. Coherence in spontaneous radiation processes. *Phys. Rev.* **93**, 99–110 (1954).
33. Navon, N., Smith, R. P. & Hadzibabic, Z. Quantum gases in optical boxes. *Nat. Phys.* **17**, 1334–1341 (2021).

Methods

Sample preparation

Around 1 billion sodium atoms are loaded into a magneto-optical trap (MOT) and transferred into a quadrupole magnetic trap with an optical plug where they are cooled by microwave evaporative cooling. Subsequently, around 10^7 atoms in the hyperfine state $|F = 2, m_F = 2\rangle$ are transferred into a single-beam 1,064 nm optical dipole trap (ODT). The beam waist and intensity of the trapping beam are controlled by a variable-size iris and an acousto-optic modulator, respectively. The beam waist was initially chosen to be large to increase the loading efficiency into a large trap volume. Because the bosonic enhancement effect requires $k_B T_c \gg E_{rec}$, the atomic gas is compressed to a higher density with a higher T_c by fully opening up the iris. Decreasing the intensity of the optical trapping beam induces evaporative cooling to a Bose–Einstein condensed cloud with around 4×10^5 atoms and around 30% condensate fraction. The final T_c can be adjusted from 6.8 μK to 11 μK by changing the final power of the optical trap. Subsequent heating of the cloud was done by sinusoidally modulating the power of the optical trapping beam by 50% at 1 kHz frequency with variable duration (from 1 ms to 49 ms).

Light scattering and collection

The probe light was generated from an independent 1,178 nm laser with frequency doubling. The frequency of the probe light was red detuned from the D2 transition of sodium by $\Delta = 25.7$ GHz. The large detuning was chosen to avoid multiple scattering of photons, to minimize the lensing effect and photo-association loss. In addition, since the detuning is much larger than the hyperfine interaction in the electronically excited state ($\Delta \gg A_{HFS} = 18.5$ MHz), the nuclear spin of the atom is preserved during the light scattering. The $1/e^2$ diameter of the probe beam is 3.3 mm in the atoms' plane. The intensity of the beam was stabilized to avoid shot-to-shot fluctuations.

Fluorescence light is collected at a 90° angle relative to the probe beam with a collection efficiency of 0.6(1)%, obtained from a calculation based on geometry, optical losses, etc. This value agrees with an experimental value derived from the laser intensity and the observed fluorescence signal at high temperatures. To detect the small number of scattered photons, we used an electron multiplying charge-coupled device (EMCCD) camera with quantum efficiency of 97% and readout noise of 3–5 electrons per pixel. Hardware binning of pixels was implemented to ensure that the photon shot noise dominates over the readout noise. Background noise was suppressed by choosing a region of interest only slightly larger than the image of the cloud.

For the light scattering in Figs. 2 and 3, at most 0.08 photons were scattered per atom. The pulse duration was 4 ms. For the data in Fig. 4, since the σ_--polarized probe light will cause optical pumping, we used weaker pulses with at most 0.03 (0.01) photons per atom for Rayleigh (Raman) scattering and a pulse duration of 3 ms.

We verified that the atoms were probed in the perturbative regime in which optical pumping and non-linear effects such as super-radiance are absent, by measuring the scattered light as a function of probe beam power (Extended Data Fig. 1). The measurement was done for both a cloud with and without BEC. The linear behaviour shows that the light scattering is indeed perturbative.

Atom count and thermometry

The atom number and temperature of the cloud (and their uncertainties) were determined from time-of-flight absorption measurements at the end of each experimental cycle. The fitting of absorption images was done using the Bose function for the thermal cloud and the Thomas–Fermi distribution for the BEC[34]. The temperature in the presence of BEC is calculated from the measured BEC fraction f by $T/T_c = (1-f)^{1/3}$.

Experimentally, the atoms were released from the trap 8 ms after the light pulse. The hold time was chosen to allow the atoms to thermalize, and was also necessary for a mechanical camera shutter to open. The shutter was necessary to block the probe beam which was collinear to the imaging beam during the light scattering. Because of the three-body loss during the light pulse and hold time, corrections are needed to obtain the atom number and temperature during the light pulse. These corrections are below 10% for most of the data. They were obtained by directly measuring the change of temperature and atom number during a few milliseconds and extrapolating this for the 10 ms delay (half the light pulse plus the hold time) in the actual experiment. For the atom number, this was done shot by shot, whereas for temperature, for robustness, we used the temperature averaged over clouds with identical preparation.

Properties of the high-density cloud

Substantial Bose enhancement of light scattering requires the critical temperature to be higher than the recoil energy. Therefore, the density n of our sample needed to be around 10^{15} cm^{-3}. Since the three-body loss rate coefficient for thermal sodium atom in $F = 2$ states at zero magnetic field is 9.6×10^{-29} cm^6 s^{-1} (ref. [35]), the estimated lifetime of the cloud ranges from 15 ms to 140 ms, depending on the temperature and trap depth. Since the typical trap frequencies in the radial (axial) direction are 9.5 kHz (290 Hz), the density drops quickly in the initial stage of time of flight and the three-body loss becomes negligible. Another consequence of the high density is the short mean free path ($l = 1/n\sigma \approx 1$ μm, where σ is the cross-section for elastic collisions). Since the typical size of the cloud is around 1 μm in the radial direction and 30 μm in the axial direction, this implies slow hydrodynamic transport in the axial direction. Due to hydrodynamic collisional effects, the equilibrium time scale in the axial direction is much slower than the trapping period and can potentially lead to non-fully equilibrated clouds in combination with fast three-body loss. More precise measurement of bosonic light scattering should therefore be done at lower densities and smaller scattering angles, or by choosing atoms with an even lower three-body loss rate (for example, ^{23}Na in the $F = 1$ state or ^{164}Dy).

Light scattering for a pure BEC and adiabatic compression

A pure Bose–Einstein condensate shows no bosonic enhancement of light scattering. We therefore studied light scattering using an almost pure condensate, and then compressed the condensate adiabatically by ramping up the power of the optical trap. An almost pure BEC could be prepared only in a shallow trap. Subsequently, the trap power was ramped up to increase the density and therefore T_c. Light scattering was measured for different final trap depths. Without compression, the photon count rate is identical to the signal for a non-degenerate thermal gas (Extended Data Fig. 2), demonstrating the absence of bosonic enhancement in a pure condensate. However, for the large values of $\kappa = 1.5$, the maximum predicted enhancement for a mixed cloud is only 9%. For higher densities, bosonic enhancement of light scattering was observed, in qualitative agreement with the theory. During compression, the cloud approximately followed the black trajectory in Fig. 2. Owing to losses and heating during compression, the condensate fraction decreased and light scattering was enhanced. Because of the heating, we were not able to map out the region of low T/T_c and low κ, where the enhancement would increase with temperature.

Theory for the bosonic enhancement factor

The bosonic enhancement factor approaches zero in the limit of low density or large recoil, $\kappa \to \infty$, and is maximized in the high-density limit $\kappa = 0$ where the normalized light scattering is given by the $S(\mathbf{q} = 0)$ at zero momentum. We now rigorously calculate $S(0)$ for power-law densities of state $g(\epsilon) = A\epsilon^x$. For a generic power-law trapping potential $V(r) \propto r^\alpha$ in d-dimensional space, the exponent x in the density of state reads[36]

$$x = \frac{d}{2} + \frac{d}{\alpha} - 1. \tag{5}$$

The box potential has $\alpha = \infty$, and in three dimensions $x = 1/2$.

Rewriting the integrals in equation (1) in terms of energy ϵ, we have

$$S(\mathbf{q}=0)=1+\frac{\int_0^\infty \mathrm{d}\epsilon\, n(\epsilon)^2 g(\epsilon)}{\int_0^\infty \mathrm{d}\,\epsilon n(\epsilon) g(\epsilon)}. \tag{6}$$

Here $n(\epsilon)=(z^{-1}\exp(\beta\epsilon)-1)^{-1}$ is the occupation number with $z=\exp(\beta\mu)$ being the fugacity and $\beta=1/k_\mathrm{B}T$.

The integrals have the following analytic solutions:

$$\int_0^\infty \mathrm{d}\epsilon\, n(\epsilon) g(\epsilon)=A\Gamma(1+x) g_{1+x}(z)/\beta^{1+x}, \tag{7}$$

$$\int_0^\infty \mathrm{d}\epsilon\, n(\epsilon)^2 g(\epsilon)=A\Gamma(1+x)(-g_{1+x}(z)+g_x(z))/\beta^{1+x}. \tag{8}$$

Here $g_n(z)$ represents the nth-order polylogarithm function. Finally, we get the following simple expression for the bosonic enhancement factor:

$$S(0)=\frac{g_x(z)}{g_{1+x}(z)}. \tag{9}$$

It can be shown that $g_x(z)/g_{1+x}(z)$ has its maximum at the BEC phase transition $z=1$. The behaviour of the polylogarithm functions at $z=1$ divides the physics into three regimes depending on the value of x. The results are summarized in Extended Data Table 1.

When $x\le 0$, both $g_x(z)$ and $g_{1+x}(z)$ diverge at $z=1$. The divergence of $g_{1+x}(z)$ implies the absence of the BEC phase transition. Therefore, $z<1$ for all temperatures, and the enhancement factor $g_x(z)/g_{1+x}(z)$ is always finite.

When $0<x\le 1$, $g_x(z)$ diverges at $z=1$ but $g_{1+x}(z)$ remains finite. This implies the presence of a BEC phase transition and (for $\kappa=0$) an unbounded light scattering rate with a divergent enhancement factor at the BEC phase transition point.

When $x>1$, both $g_x(z)$ and $g_{1+x}(z)$ remain finite at $z=1$. This implies the presence of a BEC phase transition and a bounded light scattering rate. The maximum possible enhancement factor at the transition temperature is $\zeta(x)/\zeta(1+x)$.

For the relevant case of the 3D box potential ($x=1/2$), light scattering can diverge, whereas for the 3D harmonic trapping potential ($x=2$), the maximum enhancement factor is $\zeta(2)/\zeta(3)\approx 1.37$. Extended Data Figs. 3 and 4 illustrate those cases.

To study the divergence of the enhancement factor near the phase transition for $0<x\le 1$, we now determine the behaviour for small but non-zero recoil momentum κ.

We start with the exact expression for the enhancement factor at finite recoil κ at the phase transition:

$$S(q)=1+\frac{1}{\sqrt{\pi}\Gamma(x+1/2)\zeta(x+1)}\int_0^\infty \mathrm{d}a\int_{-\infty}^\infty \mathrm{d}y\,\frac{1}{\exp(a+y^2)-1}\,\frac{a^{x-1/2}}{\exp(a+(y+\kappa)^2)-1}. \tag{10}$$

Here y represents the dimensionless momentum in the recoil direction, and a represents the total energy from all other dimensions in phase space. Since the enhancement factor diverges as κ^{2-2x} for $0<x\le 1$, we need to calculate

$$I=\lim_{\kappa\to 0}\int_0^\infty \mathrm{d}a\int_{-\infty}^\infty \mathrm{d}y\,\frac{\kappa^{2-2x}}{\exp(a+y^2)-1}\,\frac{a^{x-1/2}}{\exp(a+(y+\kappa)^2)-1}. \tag{11}$$

After transforming to polar coordinates $a=r^2\sin(\theta)^2$ and $y=-r\cos(\theta)$, one obtains $I=\lim_{\kappa\to 0}\int_0^\infty \mathrm{d}r\int_0^\pi \mathrm{d}\theta f(r,\theta)$ with

$$f(r,\theta)=\frac{\kappa^{2-2x}}{\exp(r^2)-1}\,\frac{2r(r\sin(\theta))^{2x}}{\exp(r^2-2r\kappa\cos(\theta)+\kappa^2)-1}. \tag{12}$$

We first perform the integral over r. The function $f(r,\theta)$ has a branch cut from $r=0$ to $r=+\infty$. It also has poles at $r_{\pm,n}=\kappa\cos(\theta)\pm\sqrt{-\kappa^2\sin(\theta)^2+2\pi n\mathrm{i}}$, with n being an integer. The residues at $r=r_{\pm,n}$ are

$$\mathrm{Res}\,(f(r_{\pm,n}))=\pm\frac{2\kappa^{2-2x}\sin(\theta)^{2x}}{\exp((r_\pm)^2)-1}\,\frac{(r_\pm)^{2x+1}}{r_+-r_-}. \tag{13}$$

In the limit of $\kappa\to 0$, the residues vanish if $n\neq 0$. For $n=0$, the residues remain finite:

$$\begin{aligned}\mathrm{Res}\,(f(r_{\pm,0}))&=\pm\frac{2\kappa^{2-2x}\sin(\theta)^{2x}}{\exp(\kappa^2\exp(\pm 2\mathrm{i}\theta))-1}\,\frac{(\kappa\exp(\pm\mathrm{i}\theta))^{2x+1}}{2\mathrm{i}\kappa\sin(\theta)}\\&\approx-\pm\mathrm{i}(\exp(\pm\mathrm{i}\theta)\sin(\theta))^{2x-1}.\end{aligned} \tag{14}$$

By using the Hankel contour in the complex r plane, the integral I can be related to the sum of all residues in the complex plane by

$$I(1-\exp(2\mathrm{i}\pi x))=2\pi\mathrm{i}\sum_n\int_0^\pi \mathrm{d}\theta\,\mathrm{Res}\,(f(r_{\pm,n},\theta)), \tag{15}$$

with the result:

$$\begin{aligned}I&=\frac{2\pi\mathrm{i}\int_0^\pi \mathrm{d}\theta\,(-\mathrm{i}(\exp(\mathrm{i}\theta)\sin(\theta))^{2x-1}+\mathrm{i}(\exp(-\mathrm{i}\theta)\sin(\theta))^{2x-1})}{1-\exp(2\mathrm{i}\pi x)}\\&=\frac{2\pi^2}{4^x\sin(\pi x)}.\end{aligned} \tag{16}$$

Putting all the pre-factors in, one obtains the divergent behaviour of the bosonic enhancement factor as

$$S(\kappa\to 0)\approx\frac{2\pi^{3/2}\kappa^{2x-2}}{4^x\sin(\pi x)\Gamma(x+1/2)\zeta(x+1)}. \tag{17}$$

For $0<x<1$, the divergence in equation (17) can be understood in an intuitive way. In d spatial dimensions, the first-order correlation function of the non-interacting Bose gas approaches $g^{(1)}(r)\propto 1/r^{d-2}$ at the critical point. Because the structure factor of a homogeneous sample $S_\mathrm{box}(q)$ is related to the Fourier transform of the pair correlation function $g^{(2)}(r)-1=|g^{(1)}(r)|^2\propto 1/r^{2d-4}$, $S_\mathrm{box}(q)$ diverges as κ^{d-4} when $\kappa\to 0$. For a Bose gas trapped in a power-law potential $V(r)=V_0(r/L)^\alpha$ (where L is the characteristic length of the system), only a fraction of the gas is close to local criticality at $T=T_\mathrm{c}$. This fraction can be estimated from the characteristic length scale r_0 where the trapping potential energy is similar to the recoil energy: $V_0(r_0/L)^\alpha\approx q^2/2m$. Therefore, the fraction $f\propto(r_0/L)^d\propto\kappa^{2d/\alpha}$. Qualitatively, we can treat the sample within r_0 as homogeneous and apply the result for $S_\mathrm{box}(q)$ at criticality to this small region. In the end, we get the structure factor for the trapped gas as $S(q)\propto\kappa^{2d/\alpha}\kappa^{d-4}\propto\kappa^{2x-2}$.

For $x>1$, the bosonic enhancement mainly comes from regions outside the critical region which is very small, therefore the overall enhancement factor is finite.

Density distribution

The repulsive interaction between atoms modifies the density distribution in the trapping potential and greatly reduces the overlap between the thermal cloud and the condensate. The density distribution of the cloud was obtained using the local density approximation. Locally, the Bose gas is treated as a homogeneous gas with a Hartree–Fock (HF) MF Hamiltonian[37] of

$$H_\mathrm{HF}-\mu N=-gnN-\frac{gn_0N_0}{2}+\sum_k(\epsilon_k-\mu+2gn)\,a_k^\dagger a_k. \tag{18}$$

Here n_0 represents the density of the BEC while n is the total density. μ is the chemical potential, and $g = 4\pi\hbar^2 a/m$ represents the interaction strength. N and N_0 are the total atom number and the atom number in the condensate, respectively. $a_k^\dagger$ and a_k are the creation and annihilation operators for a free particle with momentum k and kinetic energy $\epsilon_k = k^2/2m$. For a given chemical potential, the local density is obtained by solving the following pair of equations self-consistently:

$$\begin{cases} n = n_0 + \frac{1}{\lambda_t^3} g_{3/2}(e^{\beta(\mu - 2gn)}) \\ \mu = 2gn - gn_0 \end{cases} \tag{19}$$

We used an open-source package to solve these equations numerically for a harmonic trapping potential[38]. Note that here all calculations were done by assuming an isotropic harmonic trap with mean trap frequency of $\omega = (\omega_x\omega_y\omega_z)^{1/3}$. Unlike in our previous work with fermions[22], the anharmonicity corrections for bosons here are much smaller and will be neglected. Extended Data Fig. 5 shows the density profiles of a Bose gas for an ideal gas, in the semi-ideal gas approximation and HF approximation. Reference [39] discusses the differences between the three models and compares them with experimental data. The ideal gas approximation assumes no interaction between atoms. The semi-ideal gas approximation considers the interaction within the BEC and between the BEC and the thermal cloud, but not the interaction within the thermal cloud and the back-action of the thermal cloud on the condensate. The MF repulsion of the thermal cloud by the condensate substantially reduces their overlap, causing the reduction of Bose enhancement. As a comparison, the HF approximation takes all interactions into account at the MF level. The calculations in Extended Data Fig. 5 show that the back-action from the thermal cloud compresses the BEC to higher densities and further reduces their overlap by around 20%. However, the HF calculation predicts an unphysical jump in the BEC density (Extended Data Fig. 5). For modelling the density distribution in the presence of a condensate, we used the semi-ideal gas approximation since it is numerically a much simpler approach. For a fully consistent calculation of the density profiles, one would have to go beyond the HF approximation.

To understand the importance of the different interaction terms, it is useful to compare the peak density of the thermal cloud at the phase transition (n_{th}) with the peak density of the BEC at $T = 0$ (n_0). By using $n_{th} \propto N/(k_B T_c/m\omega^2)^{3/2}$ and $k_B T_c = \hbar\omega(N/\zeta(3))^{1/3}$, we get $n_{th} \propto N^{1/2}/a_{ho}^3$ (where $a_{ho} = \sqrt{\hbar/m\omega}$ is the oscillator length). For the condensate, we can use $n_0 = \mu_0/g$ with $\mu_0 = \hbar\omega(15Na/a_{ho})^{2/5}/2$ and $g = 4\pi\hbar^2 a/m$ to obtain $n_0 \propto N^{2/5}/(a^{3/5}a_{ho}^{12/5})$. Thus, the ratio of the densities of the thermal cloud and the BEC becomes $n_{th}/n_0 \propto N^{1/6}a/a_{ho}$. Although the conventional wisdom is that the density of the BEC is usually much higher than the thermal cloud, n_{th} and n_0 differ by only a factor of 2 in our experiment because of the tight confinement (Extended Data Fig. 5). Since the MF interaction of the thermal cloud has an extra factor of 2 due to the exchange term, we have a situation where the interactions in the condensate and the thermal cloud are equally important.

Pair correlation function

Atomic interactions will affect light scattering also through the pair correlation function. The exact expression for the pair correlation function for the non-interacting Bose gas reads[25]

$$G^{(1)}(r) = \sum_{l=1}^{\infty} \frac{e^{l\beta\mu}}{\lambda_t^3 l^{3/2}} e^{\frac{-\pi r^2}{l\lambda_t^2}}. \tag{20}$$

At high temperatures, the $l = 1$ term dominates, so the correlation function is a Gaussian with a correlation length $\lambda_t/\sqrt{2\pi}$. Close to the critical point, the correlation function decays exponentially with a correlation length ξ (ref. [40]):

$$g^{(1)}(r) \approx \frac{\lambda_t}{\zeta(3/2) r} e^{-r/\xi}, \quad \xi = \frac{1}{\sqrt{-2m\mu}} = \frac{\lambda_t}{\sqrt{-4\pi\beta\mu}}. \tag{21}$$

Here $g^{(1)}(r) = G^{(1)}(r)/G^{(1)}(0)$ is the normalized first-order correlation function. The correlation length ξ diverges as $|T - T_c|^{-1}$ near the critical point for the non-interacting Bose gas. Using the correlation function for the non-interacting gas, we can calculate the structure factor $S(q)$ for the ideal gas and the first-order correction of the structure factor with interactions[25], $S_{int}(q)$. Near the critical point, we obtain

$$\begin{aligned} S(q=0) &= \int_0^\infty |g^{(1)}(r)|^2 4\pi r^2 dr \propto \lambda_t^2 \int_0^\infty \frac{e^{-2r/\xi}}{r^2} 4\pi r^2 dr \\ &= 2\pi\lambda_t^2\xi, \\ S_{int}(q=0) &\approx S(q=0) - \int_{\lambda_t}^\infty |g^{(1)}(r)|^2 \frac{4a}{r} 4\pi r^2 dr \\ &\propto 2\pi\lambda_t^2\xi - 16\pi\lambda_t^2 a\Gamma\left(0, \frac{2\lambda_t}{\xi}\right) \approx 2\pi\lambda_t^2\xi - 16\pi\lambda_t^2 a \ln\frac{\xi}{2\lambda_t}. \end{aligned} \tag{22}$$

This expression shows that the relative correction due to interactions $S_{int}/S - 1 \approx -8a\ln(\xi/\lambda_t)/\xi$ vanishes as we approach the critical point. Note that the calculations were done by assuming $q = 0$ because the correction for finite momentum is quadratic in k and can be neglected.

At high temperatures, $g^{(1)}(r) \propto e^{-\pi r^2/\lambda_t^2}$ and the structure factor and its interacting correction are given by[25]

$$\begin{aligned} S(q=0) &= \int_0^\infty |g^{(1)}(r)|^2 4\pi r^2 dr \propto \int_0^\infty e^{-2\pi r^2/\lambda_t^2} 4\pi r^2 dr \\ &= \frac{\lambda_t^3}{2\sqrt{2}}, \\ S_{int}(q=0) &= S(q=0) - \int_0^\infty |g^{(1)}(r)|^2 \frac{4a}{r} 4\pi r^2 dr \\ &\propto \frac{\lambda_t^3}{2\sqrt{2}}\left(1 - 8\sqrt{2}\frac{a}{\lambda_t}\right). \end{aligned} \tag{23}$$

Therefore, the correction factor for interaction effects approaches $1 - 8\sqrt{2}a/\lambda_t$ at high temperatures. Note that the interacting pair correlation function describes the true correlation in the position of the atoms, whereas the non-interacting second-order correlation function $g_0^{(2)}(r = 0)$, which is 1 for a pure condensate and 2 for a thermal cloud, appears in the interaction parameters for the condensate and the thermal cloud, respectively[25,41].

Comparing interacting models with experimental data above the phase transition

The bosonic enhancement of light scattering is about 30% just above the phase transition temperature. The MF modification of the density distribution increases the light scattering by about 10%, whereas the modification of the pair correlation function leads to a decrease by about 10%. This is why the predictions for the full theory for interactions are close to the ideal gas prediction. This is shown in Extended Data Fig. 6, where three different models are compared with the ideal gas: (1) the MF model including only the modified density distribution of the cloud but not the pair correlation function, (2) the MF + overall suppression model that approximates the effect of the modified pair correlation as an overall reduction factor of $1 - 8\sqrt{2}a/\lambda_t$ and (3) the full interacting theory model that includes the dependence of the pair correlation function on the local chemical potential. So, we locally calculated the pair correlation function (without assuming a Gaussian or exponential form) and the structure factor $S_{int}(q)$ which gives the local scattering rate. The total light scattering rate is obtained by integrating the local rates across the cloud.

We fit the data using different models by only adjusting the overall scaling. A comparison of the χ^2 values for the fits shows that the model with only the MF interaction has the worst χ^2 (Extended Data Table 2).

Therefore, if one assumes the validity of the MF term, then our observations provide some evidence for the modification of pair correlations by interactions. Note that some of the differences in Extended Data Fig. 6a disappeared because the high-temperature asymptotic value is a fit parameter in Extended Data Fig. 6b. Unfortunately, we could not measure the asymptotic value at higher temperatures because of the limitation of the trap depth. We suggest that future experimental studies use a box potential instead of a harmonic potential to avoid the partial cancellation of MF and pair correlation effects.

Details of the interacting model below the phase transition

The full interacting theory below the phase transition becomes very complex, and we did not aim for a fully quantitative description. Therefore, we used the following approximations for the theory curves in Fig. 3b: (1) the density distribution was obtained using the semi-ideal gas approximation and (2) the effect of the pair correlation function was introduced by a reduction factor of $1-8\sqrt{2}a/\lambda_t$ (equation (23)). Note that the theory curves in Fig. 3b have no free parameters (the overall scaling being the same as in Fig. 3a).

Data availability

The data that support the plots within this paper and other findings of this study are available from the corresponding authors upon reasonable request and through Zenodo[42].

Code availability

The codes that support the findings of this study are available from the corresponding authors upon reasonable request and through Zenodo[43].

References

34. Ketterle, W., Durfee, D. S. & Stamper-Kurn, D. M. Making, probing and understanding Bose–Einstein condensates. In Bose–Einstein Condensation in Atomic Gases (eds Inguscio, M. et al.) 67–176 (IOS Press, 1999).
35. Görlitz, A. et al. Sodium Bose–Einstein condensates in the $F=2$ state in a large-volume optical trap. *Phys. Rev. Lett.* **90**, 090401 (2003).
36. Li, M., Chen, L. & Chen, C. Density of states of particles in a generic power-law potential in any dimensional space. *Phys. Rev. A* **59**, 3109–3111 (1999).
37. Pethick, C. J. & Smith, H. *Bose–Einstein Condensation in Dilute Gases* (Cambridge Univ. Press, 2008).
38. Mordini, C. hfsolver: a numerical solver for the Hartree-Fock equation of state of a homogeneous Bose gas. *Github* https://github.com/carmelom/hfsolver (2019).
39. Meppelink, R., Rozendaal, R. A., Koller, S. B., Vogels, J. M. & van der Straten, P. Thermodynamics of Bose-Einstein-condensed clouds using phase-contrast imaging. *Phys. Rev. A* **81**, 053632 (2010).
40. Proukakis, N. P., Snoke, D. W. & Littlewood, P. B. *Universal Themes of Bose–Einstein Condensation* (Cambridge Univ. Press, 2017).
41. Ketterle, W. & Miesner, H.-J. Coherence properties of Bose–Einstein condensates and atom lasers. *Phys. Rev. A* **56**, 3291–3293 (1997).
42. Lu, Y.-K. Data for figures in "Observation of bosonic stimulation in light scattering" (arXiv:2204.06639). *Zenodo* https://doi.org/10.5281/zenodo.7158468 (2022).
43. Lu, Y.-K. Code for calculations in "Observation of bosonic stimulation in light scattering" (arXiv:2204.06639). *Zenodo* https://doi.org/10.5281/zenodo.7158514 (2022).

Acknowledgements

We thank Z. Hadzibabic, J. de Hond and P. Barral for comments on the manuscript. This work is supported by NSF through the Center for Ultracold Atoms and grant no. 1506369, and from a Vannevar-Bush Faculty Fellowship.

Author contributions

All authors contributed to the concepts of the experiment, Y.-K.L. and Y.M. performed the experiment, Y.-K.L. analysed the data and performed the theoretical calculations. Y.-K.L., Y.M. and W.K. wrote the paper.

Competing interests

The authors declare no competing interests.

Additional information

Extended data is available for this paper at https://doi.org/10.1038/s41567-022-01846-y.

Supplementary information The online version contains supplementary material available at https://doi.org/10.1038/s41567-022-01846-y.

Correspondence and requests for materials should be addressed to Yu-Kun Lu.

Peer review information *Nature Physics* thanks the anonymous reviewers for their contribution to the peer review of this work.

https://doi.org/10.1038/s41567-022-01846-y

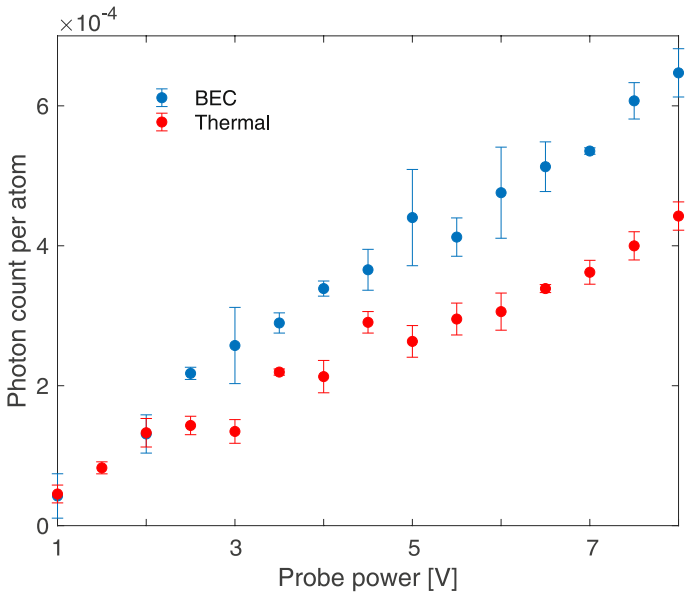

Extended Data Fig. 1 | Linearity check for light scattering. Scattered photons are measured for different probe beam powers. The blue (red) data points represent a cloud with (without) BEC. The absence of nonlinearity shows that we are working in the perturbative regime. Data points here are each averaged over 3 samples.

https://doi.org/10.1038/s41567-022-01846-y

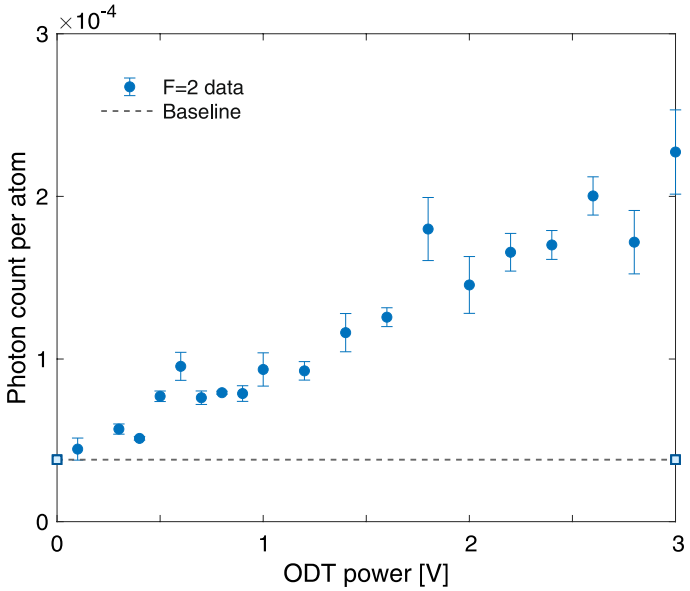

Extended Data Fig. 2 | Light scattering after compressing the cloud. The photon scattering signal was measured for different final trap depths. The dashed line represents the signal observed for a non-degenerate cloud with no bosonic enhancement. Each data point was averaged over 6 samples.

https://doi.org/10.1038/s41567-022-01846-y

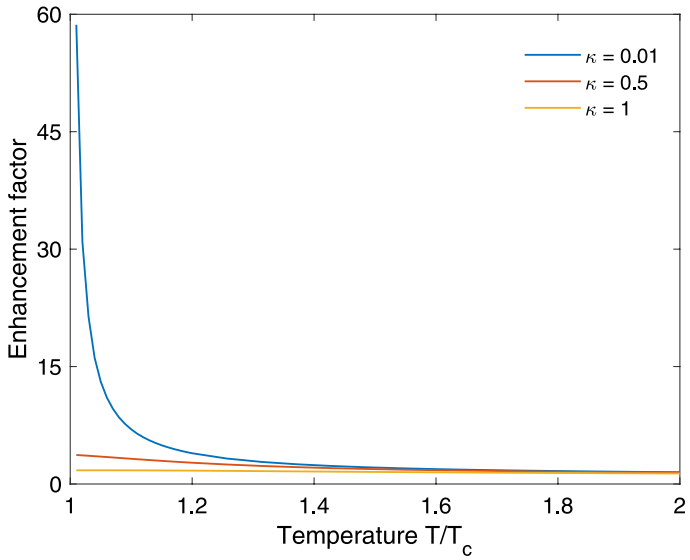

Extended Data Fig. 3 | Bosonic enhancement factor for an ideal gas in a 3D box potential for different recoil momenta κ. At the phase transition point, the bosonic enhancement factor diverges as $1/\kappa$.

https://doi.org/10.1038/s41567-022-01846-y

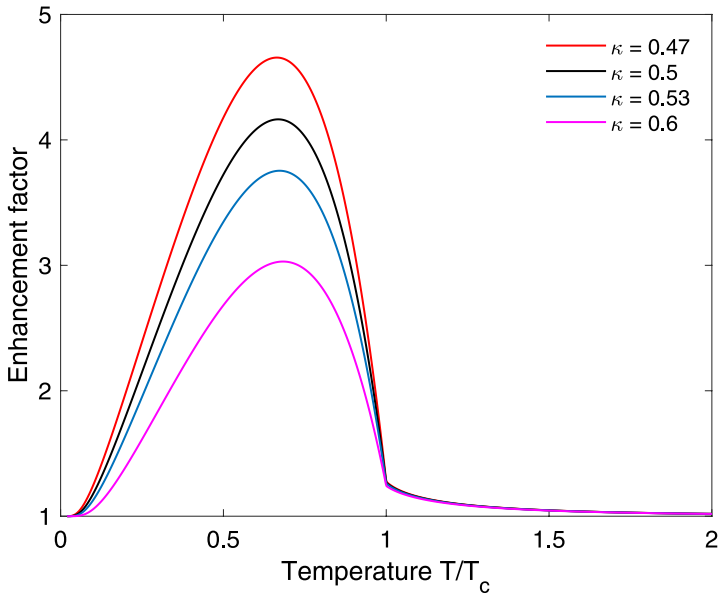

Extended Data Fig. 4 | Bosonic enhancement factor for an ideal gas in a 3D harmonic trapping potential for different recoil momenta κ. The enhancement factor is bounded at and above the phase transition, but will diverge as $1/\kappa^2$ below the phase transition.

https://doi.org/10.1038/s41567-022-01846-y

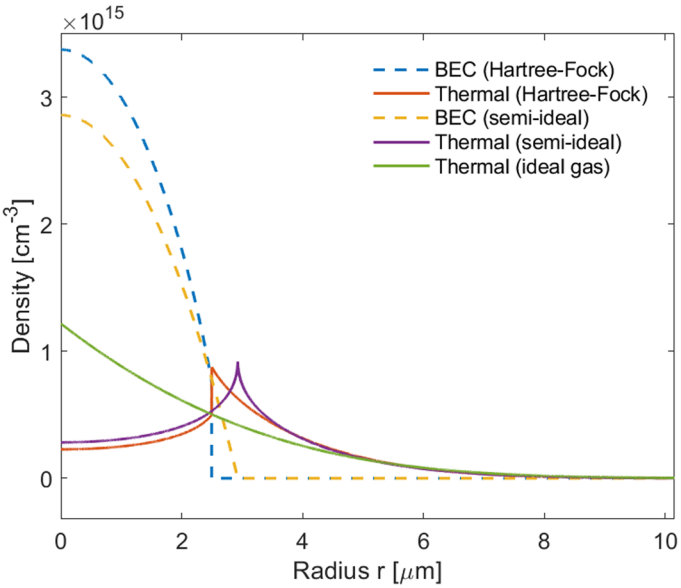

Extended Data Fig. 5 | The density distribution of the condensate and thermal cloud for different models. In the calculations we used the following values: scattering length of $a = 85a_0$ (a_0 is the Bohr radius), trap frequency $\omega = 2\pi \times 2.7$kHz, atom number $N = 4 \times 10^5$ and condensate fraction of 30%.

https://doi.org/10.1038/s41567-022-01846-y

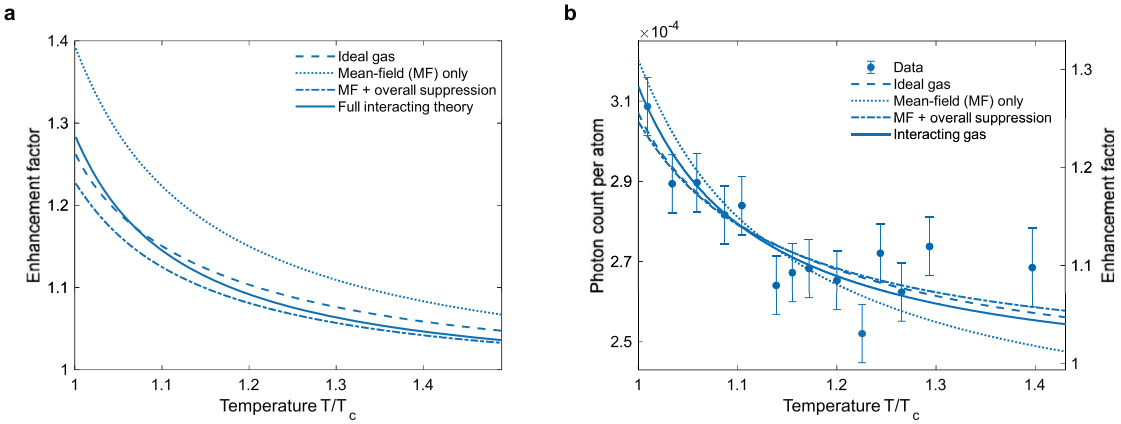

Extended Data Fig. 6 | Comparison between different models above the phase transition. (a) Predictions for the Bose enhancement factor for different models. (b) Fitting of the models to the experimental data. The only free parameter is the overall scaling. In the calculations we used the following parameters: scattering length $a = 85a_0$ (a_0 is the Bohr radius), atom number $N = 4 \times 10^5$ and dimensionless recoil momentum $\kappa = 0.51$.

https://doi.org/10.1038/s41567-022-01846-y

	$x \leq 0$	$0 < x \leq 1$	$x > 1$
BEC phase transition	No	Yes	Yes
Bosonic enhancement	Bounded	Diverges as κ^{2x-2} when $T \to T_c$	Bounded by $\zeta(x)/\zeta(1+x)$ for $T \geq T_c$

Extended Data Table 1 | Bosonic enhancement factor for different exponent *x* in the density of states. In the limit of zero recoil momentum, the enhancement factor is bounded for $x \leq 0$ and $x > 1$ while diverging for $0 < x \leq 1$.

https://doi.org/10.1038/s41567-022-01846-y

	Ideal gas	Mean-field (MF) only	MF + overall suppression	Full interacting theory
χ^2 value	13.2	21.7	12.9	13.5
Normalized χ^2 value	12.7	20.1	12.4	13
Degrees of freedom (dof)	13	13	13	13

Extended Data Table 2 | χ^2 values for fits using different models. The χ^2 values are normalized in such a way that it becomes dof = 13 for the full interacting model. As a comparison, the probability for χ^2 (dof=13) to be larger than 18.5 is 10%.